Permeable Asphalt Hydraulic Conductivity and Particulate Matter Separation With XRT

Mariana Marchioni (mariana.marchioni@polimi.it)
POLIMI: Politecnico di Milano https://orcid.org/0000-0002-6777-8090
Roberto Fedele
POLIMI: Politecnico di Milano
Anita Raimondi
POLIMI: Politecnico di Milano
John Sansalone
UF: University of Florida
Gianfranco Becciu
POLIMI: Politecnico di Milano

Research Article

Keywords: Permeable asphalt, stormwater, particulate matter, X-Ray microtomography

Posted Date: December 17th, 2021

DOI: https://doi.org/10.21203/rs.3.rs-938634/v1

Version of Record: A version of this preprint was published at Water Resources Management on March 23rd, 2022. See the published version at https://doi.org/10.1007/s11269-022-03113-4.

Abstract

Permeable asphalt (PA) is a composite material with an open graded mix design that provides a pore structure facilitating stormwater infiltration. PA is often used as a wearing course for permeable pavements and on roadways to reduce aquaplaning and noise pollution. The pore structure functions as a filter promoting particulate matter (PM) separation. The infiltrating flow characteristics are predominately dependent on pore diameter and pore interconnectivity. X-Ray microTomography (XRT) has been successfully used to estimate these parameters that are otherwise difficult to obtain through conventional gravimetric methods. The pore structure parameters allow modeling of hydraulic conductivity (k) and filtration mechanisms; required to examine the material behavior for infiltration and PM separation. Pore structure parameters were determined through XTR for three PA mixtures. The Kozeny-Kovàv model was implemented to estimate k. PM separation was tested using a pore-to-PM diameter categorical model. This filtration mechanism model was validated with data using rainfall simulation. The filtration model provided a good correlation between measured and modeled data. The identification of filtration mechanisms and k facilitate the design and evaluation of permeable pavement systems as a best management practice (BMP) for runoff volume and flow as well as PM and PM-partitioned chemical separation.

1. Introduction

The increase of urban/suburban demographics, estimated to reach 60% of the earth's population by 2025 (Heilig 2012) is resulting in increasing impervious surfaces with commensurate increases in stormwater volume and peak flow. Alterations of the microclimate caused by heat island on dense urban areas can also result on more frequent extreme rainfall events demanding a new approach on stormwater management that encourages source or near source control (Shepherd 2005, Marchioni and Becciu 2014). Diffuse constituent loads mobilized and transported by untreated stormwater discharges to receiving water is a significant driver of river and stream degradation. Water policies currently demand stormwater treatment for discharge as the EU (European Union) Water framework (2000/60/EC) and EPA (Environmental Protection Agency) Clean Water Act in the United States and local Italian regulations as the RR06-2019 of the Lombardia Region (European Commission 2000, USEPA 2018, Lombardia Region 2017).

These common conditions of the expanding built environs require adoption of stormwater management control systems that mitigates the coupled runoff volume/flow and loads. Such systems are within categories of Sustainable Urban Drainage Systems (SUDS) or LID (Low-Impact Development). Permeable pavement (PP) is categorized as a SUD or LID as a passive green infrastructure system mitigating runoff volume, flow as well as PM and PM-associated chemical loads (Marchioni and Becciu 2014, Kuang et al. 2015, Ranieri et al. 2010, Ranieri et al. 2017). Hydrologic mechanisms include infiltration, evaporation and detention storage with the pore volume and porosity of the PP base material. The PP surface retains PM as a "schmutzdecke" layer or within the pore structure of PP, thereby sequestering PM and PM-partitioned chemicals for later recovery by cleaning practices such as street sweeping (Ying and Sansalone 2010).

PA is often used as a wearing course for PP allowing vehicular traffic while acting as a stormwater control. PA is also implemented as a wearing course for conventional impervious roadways to reduce aquaplaning and noise pollution (Marchioni and Becciu 2015).

1.1. Flow through permeable porous media

A permeable pavement material can be defined as a structural matrix containing pores, connected and non-connected, dispersed within in a random or ordered geometry. A fluid can only flow through the matrix pores that are interconnected through the depth of the PP, identified as effective pores, while total porosity is composed of the total volume of connected and non-connected pores (Collins 1976). The pore structure of permeable pavement consists of a heterodisperse distribution of all pores, and depending on the mix design and pavement placement, of large interconnected pores of equivalent diameters ranging from 2 to 8 mm. (Kia et al. 2017).

Nominally, porosity (ϕ) can be defined as the fraction of the unit volume occupied by all pores. Total or absolute porosity (ϕ_T) represents the fraction of all the pores within the volume of the material while effective porosity (ϕ_e) considers only the fraction of pores that are interconnected across the depth of the PP. ϕ_e can be indexed to k (Collins 1976). For permeable pavement types such as pervious concrete and PA, ϕ_T typically ranges from 0.15 to 0.35. For permeable pavement the porosity can be determined by direct methods as density methods (Tennis et al. 2004, Montes et al. 2005, CEN 2012). XRT can be used to obtain ϕ_T, ϕ_e and pore particle size distribution (PSD_{pore}) otherwise difficult to obtain with traditional methods. An analysis on 21 pervious concrete specimens (Kuang et al. 2015) found agreement between XRT and gravimetric methods. XRT results on total porosity, effective porosity, median diameter and tortuosity were nearly independent of image resolution (Kuang et al. 2015).

Consolidation method on fresh concrete influences porosity parameters as observed by Bonicelli et al. 2013 studying pervious concrete. Kia et al. 2017 indicated that the porosity of pervious concrete was more strongly correlated with unconfined compressive strength than with k.

Hydraulic conductivity (k) is a quantitative measure of the transmission of fluid (in this case, water) through a permeable material with the fluid subject to an applied hydraulic gradient. To represent k, the sample tested must be sufficiently large to contain many pores in a representative elemental volume (Collins 1976). A measure of k depends on pore structure, effective porosity, tortuosity, pore size distribution and shape of the pores and k is also a function of compaction and mechanical alterations of the PP structure (Kia et al. 2017, Collins 1976, Kuang et al. 2015). The pore structure of the surface is critical to k.

A determination of k can be measured with direct methods in laboratory, using falling head or constant head permeameters, or in situ, normally using infiltrometers that use the principle of the falling head permeameter (Ranieri et al. 2012, Terzaghi et al. 1996, Collins 1976). The falling head permeameter yields results that are relative and comparative instead of an absolute measure of k. It is preferable to use a

constant head permeameter in the laboratory that allows a better control of the flow through PP (Ranieri, et al. 2012).

K can also be measured by indirect methods using pore parameters (Ranieri et al. 2010, Terzaghi et al. 1996). The theory of Kozeny relates the pore structure to k by considering a permeable matrix as a bundle of straight capillary tubes and then considering a solution using hydrodynamic equations for slow and steady flow. The equation was later modified to include the concept of tortuosity, considering that the tubes of flow are not straight (Collins 1976). Using a modified Kozeny-Kovàv model (KKM) as shown in Eq. 1 (Ranieri et al. 2010) compared measured and modeled saturated hydraulic conductivity (k_{sat}) results. The modified equation introduces the ϕ_e instead of ϕ_T considering thus the effective porosity that effectively contributes to permeability.

$$k_{sat} = \frac{1}{512}\frac{\gamma}{\eta}\backslash\text{varnothing}\ {}_{e}D_{e}^{2} \quad \text{Eq. 1}$$

In the Eq. 1, γ is the water specific weigh, η is the dynamic viscosity, ϕ_e is the effective porosity and D_e is the characteristic diameter. Ranieri et al. (2010) compared the results of measured k_{sat} with modeled using different diameters D_e (D_5, D_{10}, D_{15}, D_{20}, D_{30}, D_{40}, D_{50} and D_{60}) and found the best fit when using D_{30} with k_{sat} measured using a constant head permeameter.

1.2. Runoff PM load

Generation and deposition of PM by anthropogenic activities plays an important role in the partitioning and distribution of chemicals in urban areas. Hetero-disperse PM generated by anthropogenic activities, predominately traffic and urban activities function as a vector for chemical load transport by runoff. PM and chemicals from anthropogenic activities are accreted on or adjacent to impervious paved surfaces (the buildup phase) until washoff phase by hydraulic stress of runoff. The chemical load partitions to/from PM and distributes across the particle size distribution (PSD) (Ying and Sansalone 2010). PM poses as a health risk, especially the finer fraction (< 10 μm), in particular PM < 2.5 μm (European Commission 2008, IARC 2016). Vehicular traffic activities, as a main source for dry deposition PM can be correlated with indices such as average daily traffic (ADT), wind speed and direction and available surface PM load which can be further abraded by traffic into finer PM sizes (Sansalone et al. 2009). Metals (Cd, Cr, Cu, Fe, Ni, Pb and Zn) are constituents that partition and distribute across the PSD as a function of the metal, and the particle size surface area and charge. (Sansalone et al. 2009). By definition, the suspended fraction (< 25 μm) has the highest concentration of metals [mg/kg of dry PM] and is highly mobile in runoff and not retained by BMPs. In contrast the sediment fraction (> 75 mm) which is the dominant mass fraction (and therefore total surface area) transported in runoff is the PM substrate of the highest total metal mass, is readily separated in urban conveyance systems and BMPs yet is the most labile fraction (Ying and Sansalone 2010, Sansalone et al. 2009, Sansalone and Ying 2008, Sansalone and Cristina 2004, Deletic and Orr 2005). PP can function as a filter that functions as a near-source control to separate PM and chemicals from runoff. PSDs of dry deposition PM and PP pore geometric parameters are essential to design control strategies for management of PM and PM-partitioned

chemicals. If the PP is pervious concrete (in contrast to PA) the pore geometrics and surface chemistry also provide surface complexation and chemical precipitation mechanisms. While the PM filtered by the PP, whether as a schmutzdecke or deep bed deposit does act as a substrate for surface complexation, these PM reservoirs are potentially mobile unless recovered by regular maintenance and impact the driving head through the PP.

1.3. Dry deposition PM characteristics

Dry deposition PM is size (particle diameter) hetero-disperse. The median diameter (D_{50}), where 50% of particles are finer by mass, for different studies ranges from 100 to 1100 µm (Table 1). The D_{50} of runoff ((Zhang and Sansalone 2014, Ying and Sansalone 2010) was smaller than that obtained with dry deposition (154 µm versus 280 µm; 331 µm versus 97 µm). indicating that runoff did not deliver the coarser fraction. Deletic and Orr 2005 used a wet method of sampling by washing and then vacuuming to capture the suspended PM. The mean D_{50} and D_{10} over the period of a year was 397 µm and 34 µm. The D_{50} varies also with the sample position where larger particles are found mainly on the road shoulders and are more mobile with higher hydraulic stresses of runoff.

Table 1
Summary of median diameter (D_{50}) for dry deposition PM.

Watershed / Country	Sampling information	Type of surface	Sampling method	D_{50}	Reference
Abeerden, Scotland	One year average	Residential and commercial asphalt road	Washing and vacuuming	397	(Deletic and Orr 2005)
	Salting period			450	
	No salting period			361	
Bari, Italy	Cairoli Nov-2015	Residential asphalt road	Manual sweeping	111	(Ranieri. Berloco et al. 2017)
	Cairoli Jan-2016			236	
	Dante Nov-2015			268	
	Dante Jan-2016			158	
	Napoli Mar-2014	Commercial asphalt road		262	
	Napoli Jan-2016			256	
	SanGiorgi Mar-2014	Commercial porous asphalt road		1455	
	SanGiorgi Jan-2016			216	
	Tatarella Mar-2014			351	
	Tatarella Jan-2016			449	
Taranto, Italy	Cannata Mar-2014	Residential asphalt road		413	
	Cannata Dic-2015			359	
	Magna Grecia Mar-2014			331	
	Magna Grecia Dec-2015			201	
	SS7 Mar-2014	Industrial asphalt roadway		286	
	SS7 Dec-2015			378	
New Orleans, United States	Jan-2001 to Apr-2004	Asphalt road	From runoff	216	(Sansalone. Ying et al. 2009)

Watershed / Country	Sampling information	Type of surface	Sampling method	D_{50}	Reference
Baton Rouge, United States				633	
Little Rock, United States				248	
N. Little Rock, United States				587	
Cincinnati, United States				425	
Gainesville, United States	Dry periods	Asphalt parking area	Manual sweeping and vacuuming	280	(Zhang and Sansalone 2014)
Baton Rouge, United States	17 dry deposition events from Jan-Jul-2014	Asphalt roadway	Samplers	304	(Ying and Sansalone 2010) (Sansalone and Ying 2008)
Cincinnati, United States	West shoulder	Asphalt roadway	Vacuuming	500(1)	(Sansalone and Tribouillard 1999)
	East shoulder			600(1)	
	Pavement			1100(1)	

(1) D_{50} interpolated from the PM particle size distribution (PSD).

PM is a mobile, potentially labile substrate for metals and chemicals in runoff and can be physically sequestered through filtration mechanisms. A model linking metal mass and a PSD can be used to examine partitioning and distribution of metals on PM. The potential then exists to infer PP design to separate and manage a given percentage of PM-bound metal mass based on the ability to filter given PM diameters (Sansalone et al. 2009, Sansalone and Cristina 2004).

Other chemicals and microbiological species that are also present on stormwater can also partition and distribute across the PM gradation, examples include phosphorus (P), nitrogen (N) and pathogen loadings (Dickenson and Sansalone 2012, Zhang and Sansalone 2014). Zhang and Sansalone 2014 analyzed stormwater from an impervious paved car park in Gainesville, Florida (United States) and reported that dissolved N accounts for approximately 50% of N where for the particulate phase the suspended and sediment fractions showed higher N concentration (median value: 0.716 and 0.778

mg/L,) than the settleable fraction (median value: 0.298 mg/L). Based on measured data the ratio of dissolved, suspended, settleable, and sediment fraction N was approximately (to the nearest whole number) 7:2:1:3.

1.4. Filtration mechanisms

The pore mean diameter (d_m) and particle diameter (d_p) are parameters for particle filtration mechanisms. Three main mechanisms of transport can be distinguished: formation of a schmutzdecke also known as a surface (cake) generated by surficial straining, deep-bed filtration and physical-chemical filtration (Fig. 1). When the particles are relatively large compared to the media the particles does not penetrate and are retained on the surface forming a cake or a *schutzdecke*, as translated as “dirty layer” in German (Teng and Sansalone, 2004). The cake increases in thickness over time and starts behaving as a more hydraulically resistant filter, reducing the system infiltration yet also acting as a substrate for chemical surface complexation. This potential mechanism has been indexed at a $d_m/d_p < 10$ (McDowell-Boyer. Hunt et al. 1986).

Deep-bed filtration, is a result of a series of potential separation mechanisms of particles within the pore distribution of PP, occurs on the narrow range of $10 < d_m/d_p < 20$, and plays an important role in PM and chemical separation, albeit with filter ripening and failure without regular maintenance (Auset and Keller 2006, McDowell-Boyer et al. 1986). Smaller particles can only be removed by physical-chemical filtration mechanisms, normally when $d_m/d_p > 20$. In this case the mechanism depends basically on the particle diameter, whereas particles with $d_p > 5$ µm are still subject to the effect of gravitational sedimentation and $d_p < 5$ µm the effect of Brownian motion. These mechanisms have been identified for PP including pervious concrete (Teng and Sansalone 2004).

2. Objective

In this research XRT was used to obtain pore structure parameters (ϕ_T, ϕ_e, PSD_{pore}) on permeable asphalt (PA) specimens and then model k using the Kozeny-Kovàv model (KKM) and PM separation using filtration mechanisms with a categorical model of the predominant filtration mechanisms. This mechanistic filtration model was used to estimate the PM fate for the studied PA specimens relating the pore structure obtained with XRT and the PSD_{PM} comparing the results with data measured in the laboratory using a rainfall simulation. The PM loads considered were assembled based on laboratory and sampled on field. The modeled PM separation was validated with measured data using rainfall simulation.

3. Materials And Methods

3.1. Porous asphalt (PA) specimens

PA specimens were produced in the laboratory with dimension of 50 x 26 x 5 cm and 0.15. 0.20 and 0.25 nominal total porosity ($\phi_{T,Nominal}$). The $\phi_{T,Nominal}$ was obtained by maintaining the volume and varying the mass for a known bulk density. The PA hot mixture contained 4.1% by weight of a mixture of SBS (Styrene-Butadiene-Styrene) modified bitumen and a mix of 0.8/0.2 of limestone and basaltic aggregate and was compacted using a laboratory roller compactor. After the rainfall simulation tests the specimens were cut to 10 x 10 x 5 cm dimension samples to meet the XRT equipment requirements.

3.2. XRT analysis

XRT analysis used to investigate pore parameter on granular media and PP is well documented on literature (Teng and Sansalone 2004, Sansalone et al. 2008, Kuang et al. 2015). This study used a XRT NSI X25 system (NSI Inc., Rogers, MN, USA) available at Politecnico di Milano, equipped with a Dexela detector with 75 µm pixel pitch allowing for the acquisition of 1536 x 1944 pixel radiographies at full-binning with 16 bit encoding. Samples (10 x 10 x 5 cm) extracted from PA specimens molded in the laboratory representing each porosity were scanned as shown in Fig. 2. The X-ray beam was set to 110 kVp and 48 µA, and a frame-rate of 6.6 Hz was adopted together with a 13 frame-averaging (to reduce noise), leading to 1800 angular projections. From the cone-beam geometry, the estimated voxel size resulted 61.88 µm with a zoom-factor equal to 1.21. 3D tomographic reconstruction was performed using a modified Feldkamp algorithm in the version provided by efX-CT commercial software (NSI Inc.). Approximately 2.5 hours were required on a Work Station HP Z820 with 8 CPUs INTEL XEON(R) E52630 @2.6 GHz, and NVIDIA GPU GeFOrce GTX 80 Ti.

3.3. Digital image processing

For each sample approximately 800 images (with 8 Gigabyte storage) per cartesian plan (XY, XZ, YZ) were obtained. The pore structure parameters were obtained for the XY cartesian plan respecting the water flow direction used on laboratory rainfall simulation tests. The whole set of images were processed on Matlab R2016a environment. The image processing consisted on first adjusting image contrast to improve pore identification. The 16-bit greyscale images where binary (black and white images), where the solid pixels (white) represented the matrix and the black pixels represented the pores (voids). In order to measure the pores, the black and white pixels were inverted such that the solids pixels (white) represented the pores. The last step was to remove any noise that could influence results as shown in Fig. 3.

3.4. Pore parameters

The pore parameters of total porosity ($\phi_{T,XRT}$), effective porosity (ϕ_e), pore diameter, $PSD_{(pore)}$ can be used to evaluate the behavior of the porous and permeable material in the presence of fluid, solute and PM loading (Kuang et al. 2015). To obtain these parameters after image processing, the next process was to identify each pore per image by identifying a solid pixel *p* and use a flood-fill algorithm to label all the pixels connected to *p*. Each group of connections represents a pore. In Fig. 4a single pore is identified with pink color, to illustrate a sample of high connectivity.

The total porosity obtained with XRT ($\phi_{T,XRT}$) was calculated according to Eq. 2, where V_c indicates the volume for each pore, obtained by weighting on a volume basis all pores in each connection, V denotes the total volume and m is the total number of pores.

$$\emptyset_{T,XRT} = \frac{\sum_{i=1}^{m} V_{Ci}}{V} \quad \text{Eq. 2}$$

To calculate the effective porosity (ϕ_e) all the pores that didn't have pixels on the first layer (z = 0) and on the last layers scanned were excluded. Only the connected pores that went all the way through the specimens were considered. The effective porosity was computed according to Eq. 3.

$$\emptyset_{e} = \frac{\sum_{i=1}^{m} V_{Cei}}{V} \quad \text{Eq. 3}$$

In this equation V_{ce} is the volume for each effective pore connection, obtained by weighting all the connected pores in volume bases, V is the total volume of pores and m is the total number of pore connections.

For each pore in each connected region the volume and the equivalent diameters (d_m), the diameter of the circumference covering the same area as the pore, and the pore size distribution [$PSD_{(pore)}$] was obtained. The D_{30} and $D_{50;}$ the percent of pores with diameter less than 30 and 50%.

The effective porosity (ϕ_e) and pore diameter index D_{30} were used to model k using the modified Kozeny-Kovàcs based onEquation 1. Then the pore diameter index D_{50} were used combined with the $(PSD)_{PM}$ to model the particle separation according to the categorical mechanistic model for filtration.

3.5. Laboratory rainfall simulation

A rainfall simulator was designed to investigate the PM fate on porous surfaces (Andrés-Valeri, et al. 2016) (Brugin et al. 2017) (Marchioni et. al 2021). Aerial PM loading with concentrations of 0.5 kg/m^2, 1.0 kg/m^2 and 2.0 kg/m^2 were applied on the specimens that were subject to rainfall events of 50 mm/h, 100 mm/h, 150 mm/h intensities with 15-minute duration and rainfall intensity of 100 mm/h with 30 minute duration. The device collected superficial runoff and infiltrated water that were then over dried to gravimetrically quantify the PM in these flow streams. In the case of infiltrated water, due to the large volume, the measure was made by collecting three samples of the total volume and then integrating across the total volume.

3.6. Particulate Matter (PM) loads

To simulate dry deposition of PM loads in the rainfall simulation tests a mix of quarry sand and recovery fillers was assembled with a particle size distribution $(PSD)_{PM}$ that replicates real dry deposition ranging from 75 to 2000 µm and a small silt-size fraction. Traffic dry deposition PM samples were also collected on four asphalt-paved roadways in Milan (Italy). The four roads are constructed of impermeable asphalt in a highly inhabited mostly residential zone, and the samples were collected in October and November

2016 (autumn season) in the evening before cleaning (Table 2). The method used was manual sweeping on the paved road shoulders to avoid fine particles loss that might happen with vacuuming. The PSD_{PM} for the laboratory assembled mix and field samples was obtained through mechanical sieve analysis according to UNI EN 933-1. For each particle size distribution, it was determined the indices D_{10}, D_{50}, D_{60}, D_{90}, as the percent of particles finer than 10, 50, 60 and 90% and the uniformity coefficient according to Eq. 4. The cumulative mass $(PSD)_{PM}$ was modeled as a cumulative gamma distribution. The goodness of fit was verified using the Kolmogorov-Smirnov (k-s) statistics test with $p > 0,05$. The Kruskal-Wallis test with $\alpha = 0.05$ significance level was used to verify if the four different samples were statistically significantly different.

$$U = \frac{d_{60}}{d_{10}}$$ Equation 4

Table 2
Sampling sites.

Sample ID(1)	Street	Date of sampling	Land use
MI_golgi_17_ott_2016	Via Golgi	17/10/2016	Residential
MI_pascoli_21_ott_2016	Via Pascoli	21/10/2016	Residential
MI_romagna_2_nov_2016	Viale Romagna	2/11/2016	Residential Mostly
MI_zanoia_4_nov_2016	Via Zanoia	4/11/2016	Residential
(1) The samples ID follows the rule city_address_date_month_year. MI stands for Milan.			

4. Results

4.1. Pore parameters

The eight PA specimens extracted from the slabs produced in the laboratory were submitted to XRT and image analysis to obtain the pore structure parameters ($\phi_{T,XRT}$, ϕ_e, PSD_{pore}) shown in Fig. 5 and Table 3. The mean relative difference between $\phi_{T,Nominal}$ and $\phi_{T,XRT}$ was 5% and ranged from 4 to 22% while the mean relative difference from $\phi_{T,XRT}$ and ϕ_e was 6% ranging from 1 to 27% indicating a highly interconnected structure that was also visually confirmed.

The mean pore diameter mean ($d_{m,\ mean}$) ranged from 2.27 mm to 2.75 mm with 2.52 mean and 0.19 standard deviation when considering all samples of different nominal porosities ($\phi_{T,Nominal}$ of 0.15, 0.20 and 0.25). The same mix design and aggregate PSD was used for all specimens explaining the similar results for pore diameter mean for different porosities

Table 3
Pore structure parameters.

Sample ID(1)	Nominal total porosity(2) $\phi_{T,Nominal}$ [-]	Total porosity $\phi_{T,XRT}$ [-]	Effective porosity ϕ_e [-]	Pore area mean A_{mean} [mm^2]	Pore area median A_{median} [mm^2]	Pore diameter mean $d_{m,\ mean}$ [mm]	Pore diameter median D_{50} [mm]	D_{30} [mm]
PA_25_A	0.25	0,2025	0,1977	8,41	2,41	2,49	1,75	1,16
PA_25_B	0,25	0,2260	0,2202	11,74	2,58	2,75	1,81	1,19
PA_25_C	0,25	0,2130	0,2093	10,05	2,45	2,64	1,77	1,15
PA_25_D	0,25	0,2395	0,2367	13,06	1,69	2,58	1,47	0,99
PA_15_A	0,15	0,1344	0,1209	6,38	2,43	2,27	1,76	2,01
PA_15_B	0,15	0,1576	0,1484	7,53	2,48	2,40	1,78	1,16
PA_15_C	0,15	0,1370	0,1006	6,41	2,44	2,30	1,76	1,21
PA_20	0,20	0,2432	0,2472	12,92	2,46	2,74	1,77	1,22
(1) The samples ID follows the rule MATERIAL_NOMINAL TOTAL POROSITY_SAMPLE NUMBER								

Obtained with bulk density.

Figure 6 illustrates the PSD_{pore} on pore diameter (d_m) basis for each PA sample as a probability density function (PDF) and cumulative density function (CDF). The d_m ranged from 0.75 mm to 12 mm with a mean $D_{50}$of 1.88 mm for all samples and D_{90} of 5.25 mm for all samples with the exception of PA_15_A with a D_{90} of 7.25 mm.

4.2. Modeled saturated hydraulic conductivity (k_{sat})

The KKM proposed by Ranieri et al. (2010) was used to determine k_{sat} using the pore diameter (D_{30}) obtained with XRT and image analysis (Table 4). The results range from $2.88x10^{-4}$ to $7.21x10^{-4}$ m/s where the lowest k_{sat} was observed for the specimen with $\phi_{T,Nominal}$ = 0.15. Soils as granular matrices with hydraulic conductivity within this range are considered having good drainage properties (Terzaghi et al. 1996).

Table 4
– Modeled saturated hydraulic conductivity, $k_{sat,modeled}$.

Sample ID	Effective porosity ϕ_e [-]	D_{30} [mm]	$k_{sat\ modeled}$ (m/s)
PA_25_A	0.20	1.16	5.21×10^{-4}
PA_25_B	0.22	1.19	6.06×10^{-4}
PA_25_C	0.21	1.15	5.42×10^{-4}
PA_25_D	0.24	0.99	4.50×10^{-4}
PA_15_A	0.12	2.01	9.54×10^{-4}
PA_15_B	0.15	1.16	3.91×10^{-4}
PA_15_C	0.10	1.21	2.88×10^{-4}
PA_20	0.25	1.22	7.12×10^{-4}

4.3. PM loads characteristics

Table 5 and Fig. 7 shows $(PSD)_{PM}$ results from the PM loads used in the laboratory rainfall simulation tests and collected from the field. Higher values of D_{50} compared with D_{50} from previous studies are shown in Table 1, where the mean D_{50} regardless of sampling method was 408 mm and median 351 mm. Comparing the laboratory and field samples using the Kruskal-Wallis test indicated that the five samples did not show a statistically significantly difference between PSDs for a p-value = 0.8892 with 95% confidence level.

The gravimetric PSD was modeled as a cumulative gamma distribution with a goodness of fit verified using the Kolmogorov-Smirnov (k-s) statistics test with ($p > 0.05$) (Table 6).

Table 5
– PM load characteristics

Sample ID	d_{10}	d_{50}	d_{60}	d_{90}	U
	[µm]	[µm]	[µm]	[µm]	[-]
Laboratory assembled mix	189	1906	3347	9593	18
MI_golgi_17_ott_2016	185	1767	2502	6794	13.5
MI_pascoli_21_ott_2016	75	1150	1732	5954	23.1
MI_romagna_2_nov_2016	75	738	1092	3862	14.6
MI_zanoia_4_nov_2016	89	524	715	1780	8.0

Table 6
– Cumulative particle size distribution $(PSD)_{PM}$ modelling parameters.

Sample ID	Gamma distribution			Goodness of fit(1)		
	α	β	SSE	p-value	K-S	Hyp. Null(2)
Laboratory assembled mix	0.59	6.74	102	1.0000	0.0909	true
MI_golgi_17_ott_2016	0.80	3.45	36.35	0.9448	0.1667	true
MI_pascoli_21_ott_2016	0.57	3.89	142.05	0.3874	0.2941	true
MI_romagna_2_nov_2016	0.56	2.57	284.39	0.3874	0.2941	true
MI_zanoia_4_nov_2016	1.09	0.66	307.97	0.3874	0.2941	true

(1) Fit of the cumulative gamma distribution.

(2) Null hypothesis that the samples are drawn for identical distribution ($p > 0.05$). True or false.

4.4. Measured particle separation

PM fate measured from the laboratory physical modeling elucidated the PM mass retained on the PA specimens (as a schmutzdecke) and within the specimens as deep bed filtration (specific deposit), exfiltrated through the specimen or washed off the specimens through the hydraulic stress of runoff. Figure 8 and Table 7 illustrates the PM fate for PA specimens load with 0.5 kg/m^2 and 2.0 kg/m^2. PM subject to a 100 mm/h rainfall with 30 minutes duration and 150 mm/h and 15 minutes duration and also 2.5 and 7.0% slope. The majority (> 85%) of the PM load was retained on the specimen surfaces as a schmutzdecke and within the pore matrix of the specimens. For the test conditions the schmutzdecke formation did not increase volumetric runoff substantially; remaining below a volumetric runoff coefficient of 0.20 (Andrés-Valeri 2016). Less than 15% was exfiltrated through the specimens and consisted of fine suspended PM. The portion of PM loads that exfiltrated through the specimen could

potentially reach subgrade below the PA pavement structure, where the inclusion of a geotextile could retain these exfiltrated particles if required. A nominal fraction of PM (< 2% on a gravimetric basis) was washed off with runoff indicating that for the test conditions that the use of PA reduce PM loads that reach the drainage system.

Increasing PM load also increase the PM mass retained on the specimen as the schmutzdecke formed on the surface due to progressive filtration by the schmutzdecke to retain finer suspended PM that otherwise would pass into and through the PA with the potential of exfiltration of suspended PM as PM-partitioned chemicals to subgrade. Given that there was not a significant increase of the runoff PM mass and neither the volumetric runoff coefficient indicates that the schmutzdecke acts to improve the retention of PM without impacting runoff reduction and therefore benefits the permeable pavement service life. By increasing slope or rainfall intensity a slight increase on runoff volume that washed off part of the PM that otherwise would be retained on the specimen, consequently increasing PM mass on runoff (Table 7).

Table 7
PM fate by percent of mass on different conditions on rainfall simulation tests.

Rainfall intensity [mm/h]	Duration [min]	Slope	Aerial loading [kg/m^2]	Total Porosity $\phi_{T,nominal}$	PM fate on mass		
					% runoff	**% leached**	**% cake + straining**
100	30	2.5%	0.5	0,15	0.64%	9.38%	89.99%
				0,20	0.96%	7.14%	91.90%
				0,25	0.64%	8.66%	90.70%
			2	0,15	0.70%	4.90%	94.40%
				0,20	0.62%	4.42%	94.96%
				0,25	0.52%	3.63%	95.86%
		7%	0.5	0,15	1.41%	10.67%	87.92%
				0,20	1.02%	11.44%	87.53%
				0,25	1.16%	10.70%	88.14%
			2	0,15	7.28%	3.12%	89.60%
				0,20	1.50%	4.12%	94.38%
				0,25	0.85%	4.56%	94.58%
150	15	2.5%	0.5	0,15	0.66%	8.01%	91.33%
				0,20	0.73%	8.48%	90.79%
				0,25	0.37%	9.27%	90.36%
			2	0,15	4.68%	2.04%	93.28%
				0,20	0.58%	3.70%	95.72%
				0,25	0.80%	5.09%	94.11%
		7%	0.5	0,15	0.98%	4.88%	94.13%

4.5. Modeled PM separation

The categorical mechanistic model considering that the ratio d_m/d_p governs the PM fate was applied for the laboratory physical model and field PM and compared with the PM fate obtained with the rainfall simulator for validation. The d_m considered was the mean pore diameter ($d_{m,\,mean}$) obtained through XRT for each sample (Table 3) while d_p came from the $(PSD)_{PM}$. For the laboratory PM gradation most of the PM mass (83.1–88.5%) was retained on the PA surface forming a schmutzdecke (Table 8). In this scenario the PM is easily recovered through standard maintenance practices such as using vacuuming

devices. The percent of mass that was filtered in the pore space through physical-chemical parameters, and therefore could potentially exfiltrate to the subgrade, ranged from 7.6 to 11.3%. The measured and modeled data presented a maximum of 8% of relative percent difference. The simple categorical mechanistic model presented representative results under the test conditions.

Table 8
Modeled dominant filtration mechanism for the laboratory PM assembled mix on mass.

Sample ID	PM fate on mass		
	Physical-chemical	Straining	Cake
PA_25_A	8.4%	4.2%	87.4%
PA_25_B	8.5%	4.3%	87.1%
PA_25_C	8.4%	4.2%	87.3%
PA_25_D	7.6%	3.8%	88.6%
PA_15_A	11.3%	5.6%	83.1%
PA_15_B	8.4%	4.2%	87.4%
PA_15_C	8.4%	4.2%	87.4%
PA_20	8.6%	4.3%	87.0%

The categorical mechanistic model was then applied for the field dry deposition PM samples. For all the PA samples, 87% of the PM mass was retained on the specimen surface creating a schmutzdecke. The percent of PM mass that was retained through deep bed filtration was 5% for the PA_20 (0.20 porosity) 10% for the PA_25 (0.25 porosity) and 8% for the PA_15 (0.15 porosity).

The percent of PM mass that was potentially detained only by physical-chemical mechanism allowing for potential exfiltration was 7% for the PA_20 (0.20 porosity) 3% for the PA_25(0.25 porosity) and 3% for the PA_15 (0.15 porosity). The results depend on the d_m and not on the total porosity which can explain equivalent results for different total porosity and less PMl passing through the $\phi_{T,nominal}$ = 0.25 porosity specimen than the $\phi_{T,nominal}$ = 0.15 specimen. This can also explain the similar results for filtration mechanisms since d_m governed filtration mechanism for the same index of mean pore diameters.

5. Conclusions

The growing urbanization scenario demands a comprehensive stormwater management emphasizing source control for runoff, PM and chemicals. Such solutions move beyond conventional conveyances of stormwater from one point to another location downstream. PM accumulated on pavement surfaces is mobilized by hydraulic stresses after the buildup phase and is transported in stormwater into drainage

systems becoming a source of impairment for receiving waters. Permeable pavement systems using permeable surface materials such as pervious concrete and permeable asphalt (PA) provides stormwater infiltration reducing runoff and act as a filter promoting PM and chemical load removal. This type of control system is an established technology that is market-available and amenable to design, regulations and standards. Current research focuses on materials characteristics, modelling and improves overall performance

This research used rainfall simulation, X-Ray microTomography (XRT) and field material sampling to investigate aspects of PM separation by PA. Pore structure parameters (total porosity, effective porosity, pore size distribution) that are complex or not possible to obtain through conventional methods were obtained through XRT. Once a methodology was established for image analysis obtained with XRT these parameters were quantified. However, the method is still a research method and needs further development for applications outside of the research environment. The ϕ_T results were in accordance with the ones obtained through bulk density. The ϕ_T and ϕ_e, both obtained through XRT, presented a mean relative difference of 6% and results were confirmed by visual observation of the highly interconnected pores.

The modeling of k results confirmed that the PA samples are suitable to allow stormwater infiltration presenting k values similar to a well-drained granular soil. The filtration mechanisms were investigated by physical modeling and using a categorical mechanistic model based on pore and particle diameter. For the studied specimens and loads the dominant mechanism was the accumulation on surface, namely a schmutzdecke or surface cake of PM which provided progressive filtration and protection of the PA. Most of PM (> 85%) remained on the porous surface with a much smaller fraction subject to deep-bed filtration for both the laboratory PM mix and the samples obtained on field. This “cake” leads to a nominal k reduction while functioning by also retaining finer suspended PM over time that otherwise would pass through and be exfiltrated from the PA. Hence, as the schmutzdecke forms PM and chemical separation is improved with time. The “cake” can be easily removed through conventional maintenance.

In conclusion, this research investigates PA normally used for permeable pavement system through a physical modeling program of rainfall simulation, XRT and k and filtration mechanism modelling. The filtration mechanism model showed good accordance between measured and modeled results. A Computational Fluid Dynamics (CDF) model using iterations of the pore structure and PM granulometric indices could give more accurate view of filtration mechanism and chemical load fate. A combination of parameter studied by this research could be used to develop a model to predict PM separation and define maintenance routines and could be a follow up of this research.

Declarations

Acknowledgments

The authors acknowledge the contribution of the Eng. Matteo Brugin and Eng. Martina Ceriani through their graduation thesis, the AMALA laboratory at Politecnico di Milano and Capes for funding this work through the scholarship number BEX 9224/13-0.

Conflict of Interest: The authors declare that they have no conflict of interest.

Ethical approval: not applicable.

Consent to Participate: not applicable.

Consent to Publish: not applicable.

Authors Contributions. Conceptualization: M. Marchioni, R. Fedele, J. Sansalone, G. Becciu. Methodology: M. Marchioni, R. Fedele, J. Sansalone, G. Becciu. Formal analysis and investigation: M. Marchioni, R. Fedele, J. Sansalone, G. Becciu. Writing - original draft preparation: M Marchioni. Writing - review and editing: M. Marchioni, A. Raimondi. Supervision: G. Becciu.

Funding: Capes through the scholarship number BEX 9224/13-0.

Competing Interests: not applicable.

Availability of data and materials: Authors agree with data transparency and undertake to provide any required data and material.

References

1. Andrés-Valeri VC, Marchioni M, Sañudo-Fontaneda LA, Giustozzi F, Becciu G (2016) Laboratory assessment of the infiltration capacity reduction in clogged porous mixture surfaces. Sustainability 8(8):751
2. Auset M, Keller AA (2006) "Pore-scale visualization of colloid straining and filtration in saturated porous media using micromodels." Water resources research 42(12)
3. Bonicelli A, Crispino M, Giustozzi F, Shink M (2013) "Laboratory Analysis for Investigating the Impact of Compaction on the Properties of Pervious Concrete Mixtures for Road Pavements". Adv Mater Res 723:409–419
4. Brugin M, Marchioni M, Becciu G, Giustozzi F, Toraldo E, Andrés-Valeri VC (2017) "Clogging potential evaluation of porous mixture surfaces used in permeable pavement systems." European Journal of Environmental and Civil Engineering: 1–11
5. CEN EC, f. S (2012) Bituminous Mixtures-Test method for hot mix asphalt Part 6: Test methods for hot mix asphalt. Determination of bulk density of bituminous specimens. BS EN 12697-6:2012
6. Collins RE (1976) "Flow of fluids through porous materials."
7. Deletic A, Orr DW (2005) Pollution buildup on road surfaces. J Environ Eng 131(1):49–59

8. Dickenson JA, Sansalone JJ (2012) Distribution and disinfection of bacterial loadings associated with particulate matter fractions transported in urban wet weather flows. Water Res 46(20):6704–6714
9. European Comission (2000) Directive 2000/60/EC of the European Parliament and of the Council of 23 October 2000 establishing a framework for community action in the field of water policy.Off. J. Eur. Communities
10. European Comission (2000) Directive 2008/50/EC on ambient air quality and cleaner air for Europe. Off. J. Eur. Communities
11. Heilig GK (2012) "World Urbanization Prospects: The 2011 Revision." United Nations, Department of Economic and Social Affairs (DESA), Population Division. Population Estimates and Projections Section, New York
12. IARC Working Group on the Evaluation of Carcinogenic Risks to Humans (2016) Outdoor Air Pollution. IARC Monographs on the Evaluation of Carcinogenic Risks to Humans, 109, 9
13. Kia A, Wong HS, Cheeseman CR (2017) Clogging in permeable concrete: A review. J Environ Manage 193:221–233
14. Kuang X, Ying G, Ranieri V, Sansalone J (2015) Examination of Pervious Pavement Pore Parameters with X-Ray Tomography. J Environ Eng 141(10):04015021
15. Lombardia Region (2017) Regolamento Regionale 23 novembre 2017, n. 7. Regolamento recante criteri e metodi per il rispetto del principio dell'invarianza idraulica ed idrologica ai sensi dell'articolo 58 bis della legge regionale 11 marzo 2005, n. 12 (Legge per il governo del territori
16. Marchioni M, Becciu G (2015) "Experimental Results On Permeable Pavements In Urban Areas: A Synthetic Review. " International Journal of Sustainable Development Planning 10(6):806–817
17. Marchioni ML, Becciu G (2014) "Permeable pavement used on sustainable drainage systems (SUDs): a synthetic review of recent literature. " WIT Press Urban Water II, p 12
18. McDowell-Boyer LM, Hunt JR, Sitar N (1986) Particle transport through porous media. Water Resour Res 22(13):1901–1921
19. Montes F, Valavala S, Haselbach LM (2005) A new test method for porosity measurements of Portland cement pervious concrete. J ASTM Int 2(1):1–13
20. Ranieri V, Antonacci M, Ying G, Sansalone J (2010) "Application of Kozeny-Kovàcs model to predict the hydraulic conductivity of permeable pavements." Transportation Research Record: Journal of the Transportation Research Board(2195): 168–176
21. Ranieri V, Berloco N, Colonna P, Fedele V, Sansalone JJ (2017) Granulometry of Particulate Matter Recovered from Roadway Systems in Apulia. Transportation Research Board 96th Annual Meeting. T. R. B. (TRB). Washington DC, United States
22. Ranieri V, Colonna P, Sansalone J, Sciddurlo A (2012) "Measurement of hydraulic conductivity in porous mixes." Transportation Research Record: Journal of the Transportation Research Board(2295): 1–10

23. Sansalone J, Cristina C (2004) Gradation-based metal mass prediction utilizing granulometry of snow particulate residuals. J Environ Eng 130(12):1488–1497.1410
24. Sansalone J, Ying G (2008) Partitioning and granulometric distribution of metal leachate from urban traffic dry deposition particulate matter subject to acidic rainfall and runoff retention. Water Res 42(15):4146–4162
25. Sansalone J, Tribouillard T (1999) "Variation in characteristics of abraded roadway particles as a function of particle size: implications for water quality and drainage." Transportation Research Record: Journal of the Transportation Research Board(1690): 153–163
26. Sansalone J, Ying G, Lin H (2009) Distribution of metals for particulate matter transported in source area rainfall-runoff. J Environ Eng 136(2):172–184
27. Sansalone J, Kuang X, Ranieri V (2008) Permeable pavement as a hydraulic and filtration interface for urban drainage. Journal of irrigation drainage engineering 134(5):666–674
28. Shepherd JM (2005) A review of current investigations of urban-induced rainfall and recommendations for the future. Earth Interact 9(12):1–27
29. Teng Z, Sansalone J (2004) "In situ partial exfiltration of rainfall runoff. II: Particle separation" Journal of environmental engineering 130(9):1008–1020
30. Tennis PD, Leming ML, D. J. Akers and N. R. M. C. Association (2004) Pervious concrete pavements, Portland Cement Association Skokie, IL
31. Terzaghi K, Peck RB, Mesri G (1996) Soil mechanics in engineering practice. John Wiley & Sons
32. USEPA (2018) The Clean Water Act (CWA). United States Envirommental Agency
33. Ying G, Sansalone J (2010) Transport and solubility of Hetero-disperse dry deposition particulate matter subject to urban source area rainfall–runoff processes. Journal of hydrology 383(3–4):156–166
34. Zhang H, Sansalone J (2014) Partitioning and first-flush of nitrogen in rainfall-runoff from an urban source area. J Environ Eng 140(8):04014027

Figures

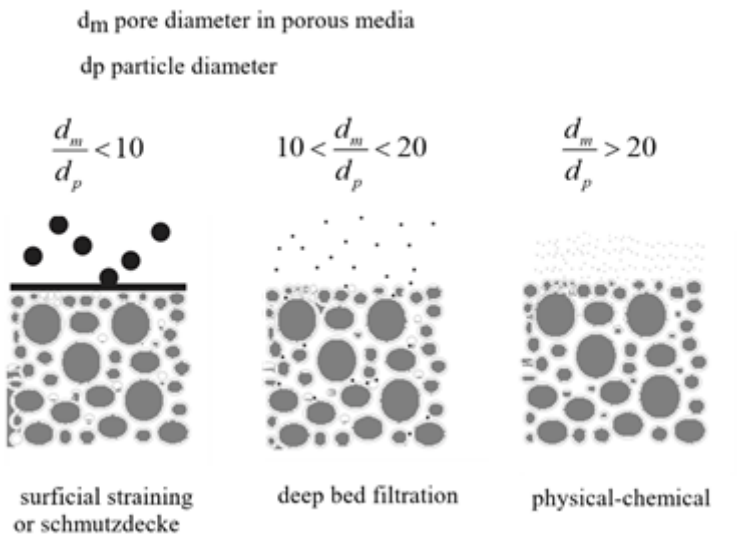

Figure 1

Filtration mechanism in permeable pavement systems.

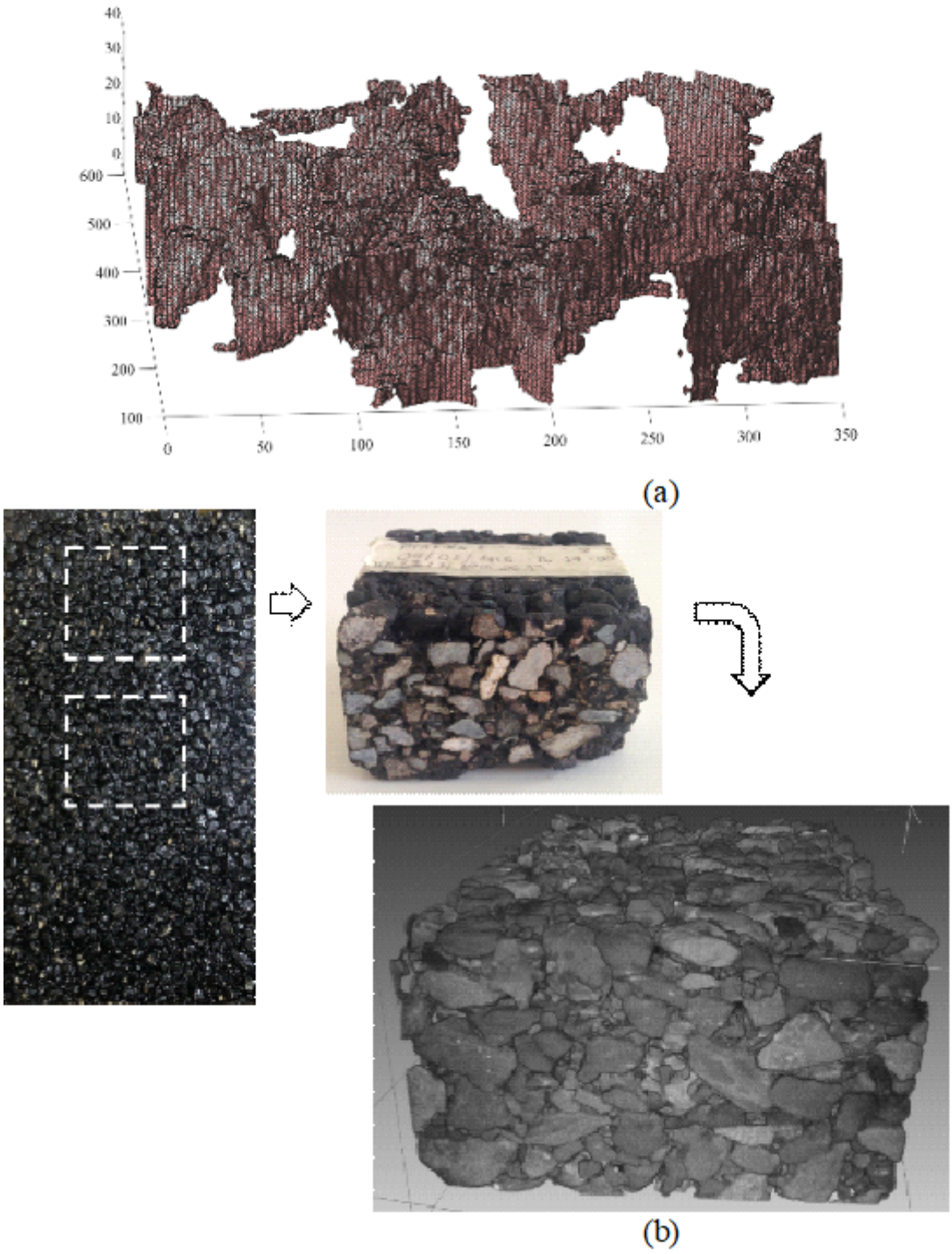

Figure 2

(a) Illustration of PA specimen, (b) sample extruded for the XRT and 3D reconstruction of the connected porosity network in a small sub volume of the sample.

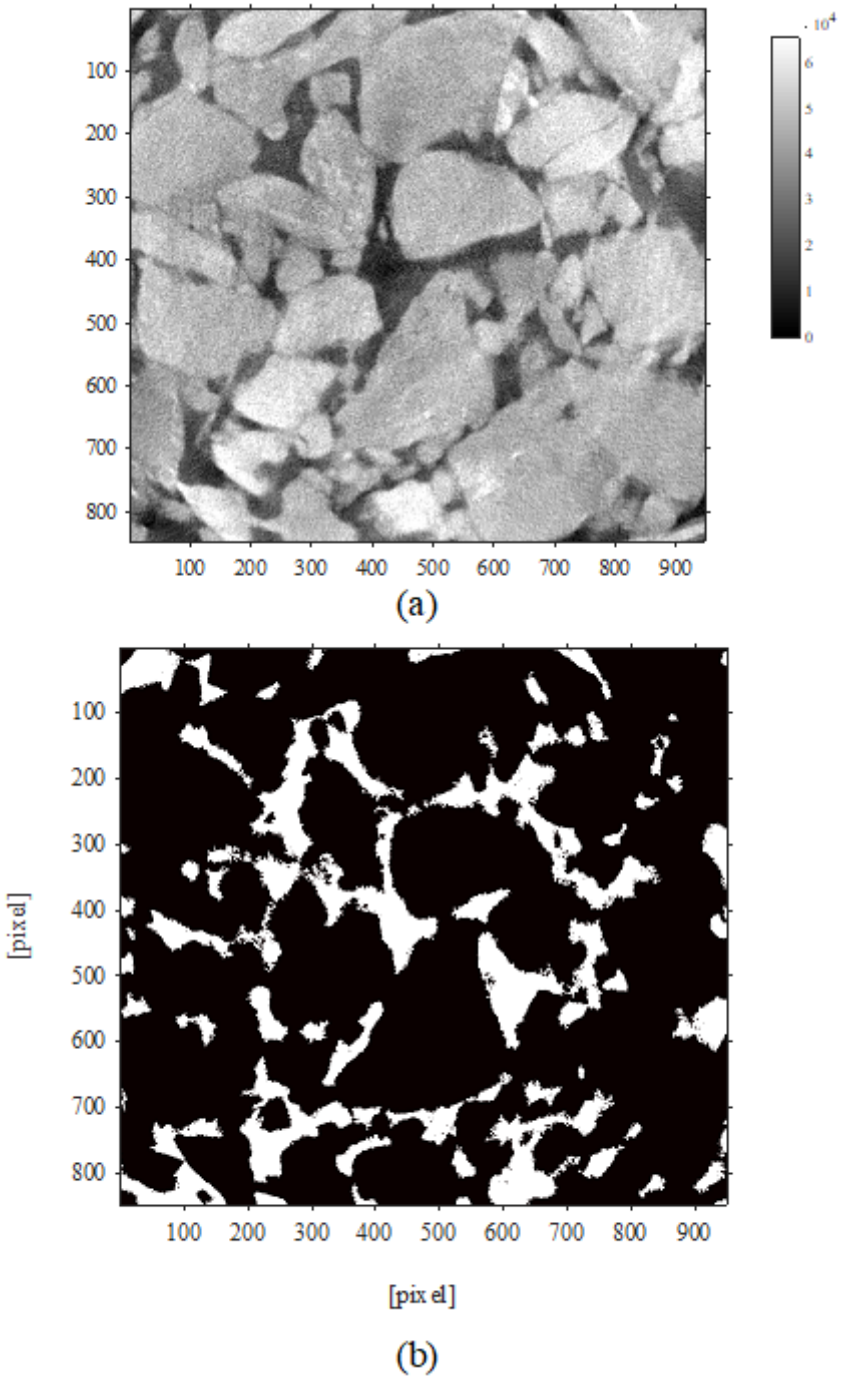

Figure 3

(a) Original image acquired with the XRT and (b) binary image used in the analysis, where the white pixels represent the pores.

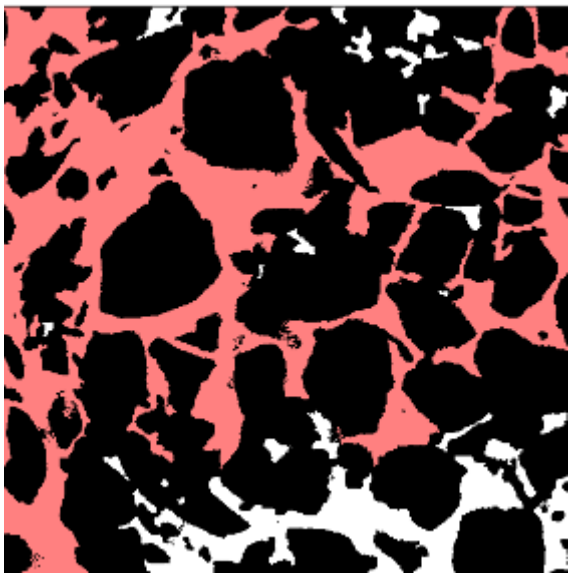

Figure 4

Pore identification for a sample layer.

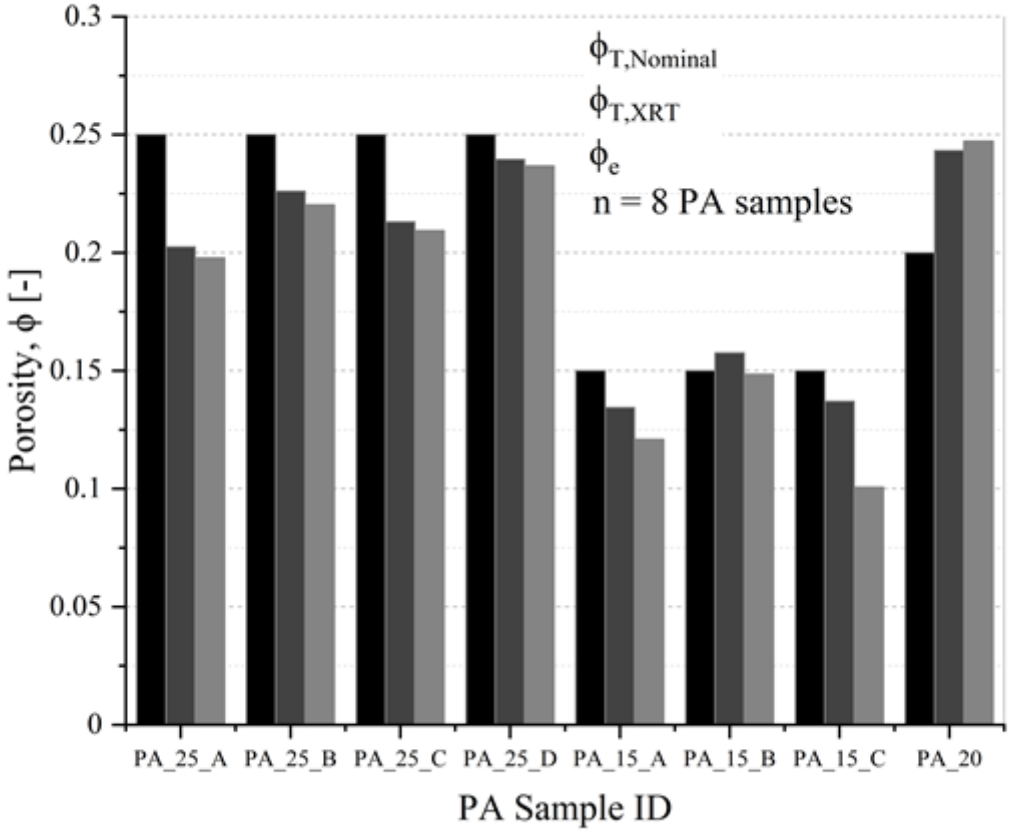

Figure 5

Nominal total porosity ($\phi_{T,Nominal}$), total porosity obtained with XRT ($\phi_{T,XRT}$) and effective porosity (ϕ_e) for PA samples.

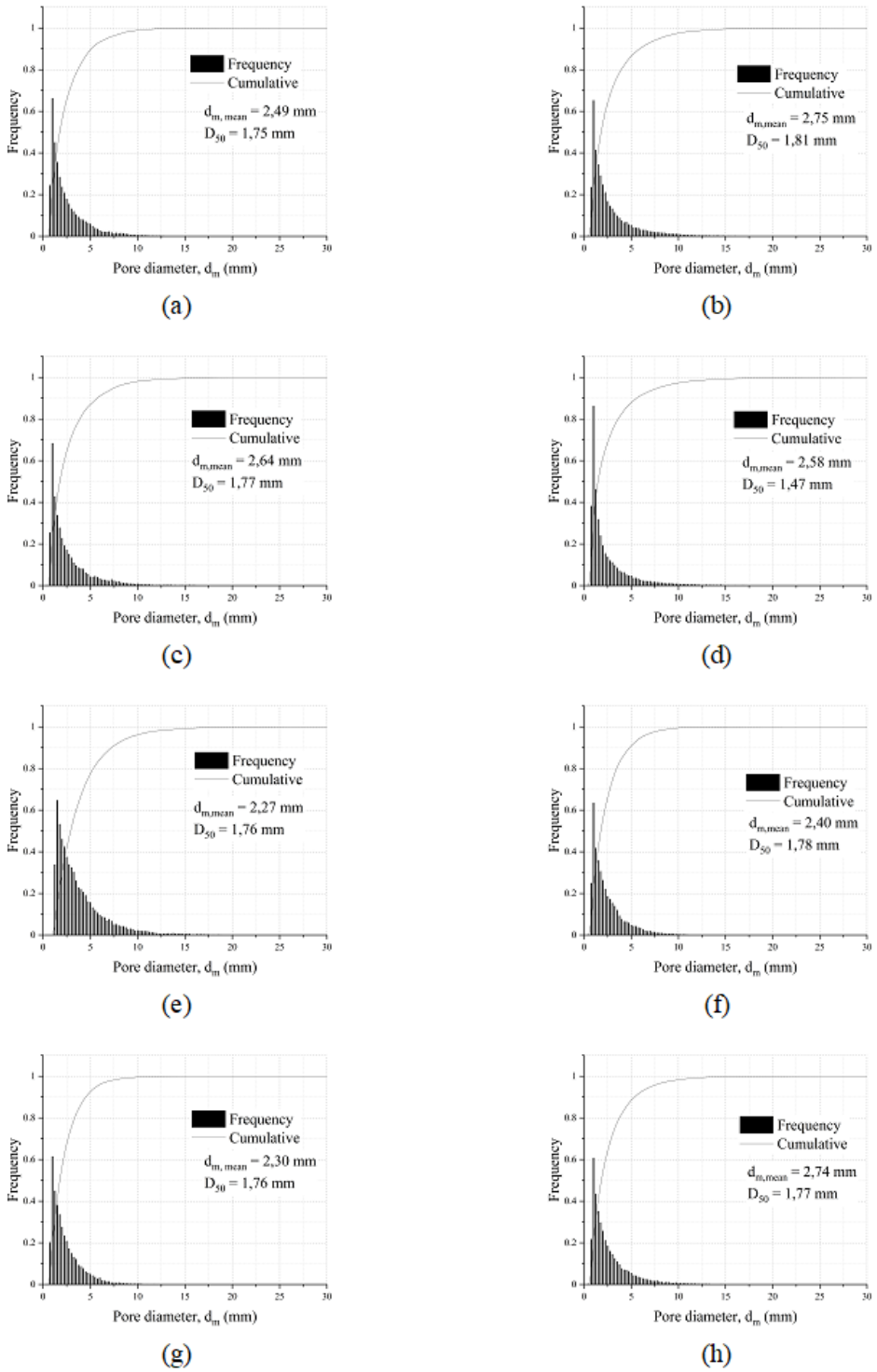

Figure 6

PSD_{pore} obtained with XRT and image analysis. (a) – PA_25_A, (b) – PA_25_B, (c) – PA_25_C, (d) - PA_25_D, (e) – PA_15_A, (f) – PA_15_B, (g) – PA_15_C, (h) – PA_20.

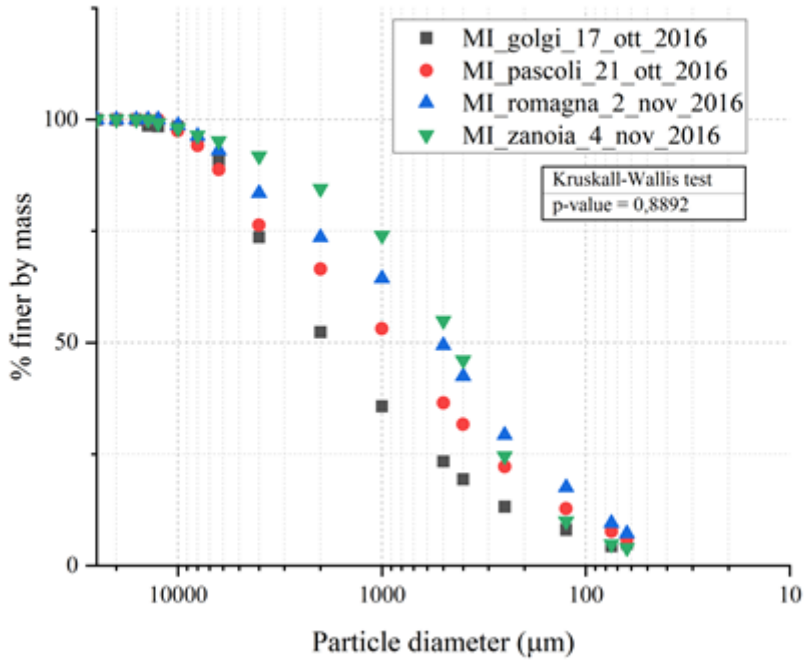

Figure 7

Particle size distribution of dry deposition $(PSD)_{PM}$ collected in Milan. Italy.

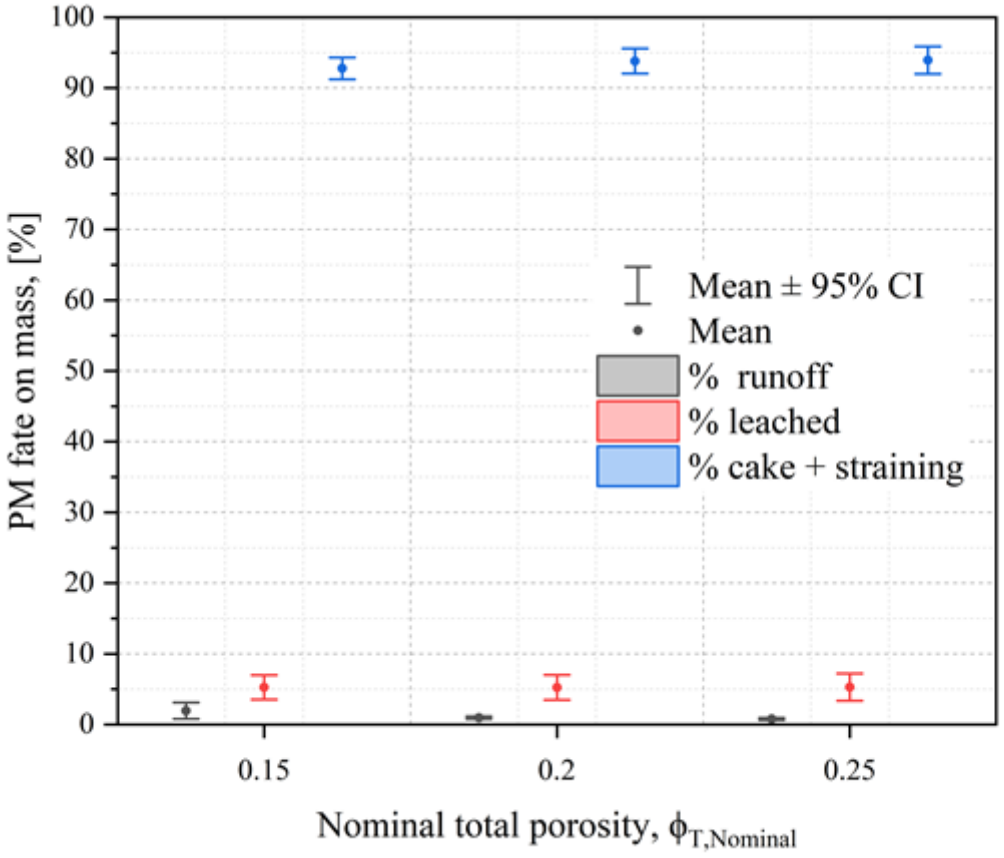

Figure 8

PM fate on mass for PA specimens for various rainfall and load conditions.